Trans. JSASS Aerospace Tech. Japan
Vol. 14, No. ists31, pp.Pd_1 - Pd_9, 2017

An Electromagnetically Actuated, Self-Reconfigurable Space Structure

By Martin NISSER,[1)] Dario IZZO,[1)] and Andreas BORGGRAEFE[1)]

[1)]*Advanced Concepts Team, European Space Agency, Noordwijk, The Netherlands*

(Received April 16th, 2017)

The growing performance and miniaturization of commercial off-the-shelf components and space technology suggests a future in which large swarms of miniature spacecraft could be used for the on-orbit formation of reconfigurable space structures. This paper presents a cubic spacecraft based on the PocketQube and demonstrates how two such spacecraft can pivot with respect to each other by actively controlling the strength and polarity of electromagnets embedded along their edges. By first aggregating eight spacecraft in a target configuration using a distributed path planning technique, a simulation of the full multibody dynamics is used to demonstrate the ability of the electromagnetic actuators to reconfigure the collective into a target configuration.

Key Words: Smart Structures, Swarm Robotics, Self-Assembly, Programmable Matter

Nomenclature

F	:	Force
$\mathrm{d}l$	:	Infinitesimal length
r	:	Distance
m	:	Mass
U	:	Control input
t	:	Time
e	:	Error
k_p	:	Proportional gain
k_d	:	Derivative gain
k_i	:	Integral gain
C	:	Electromagnet
v	:	Spacecraft velocity
P	:	Spacecraft position
ζ	:	Target position
I	:	Current

1. Introduction

Space structures traditionally aim at carrying out a single task, such as trusses, booms or scaffolds used for the one-time deployment of solar panel arrays. While these structures can be modular to permit assembly into larger structures, the final assemblies are permanent and cannot be re-configured for other purposes. In order to perform many different tasks, missions today require the integration of many expensive dedicated structures and devices. Future low-cost missions will require spacecraft to adapt to different tasks and respond to unforeseen events, such as the unsuccessful deployment of a solar array. In addition, the realization of future large space telescopes will require either precise formation flying or in-orbit assembly.[1,2)]

Structures capable of morphological adaptation would address many challenges associated with today's limitations on launch mass and volume, as well as facilitating stowage during launch. Reconfigurable structures could realize new functionality such as the formation of temporary structures to aid in spacecraft inspection and astronaut assistance, actively changing their inertia properties, and enabling replacement or augmentation of the structure with additional modules over multiple launches.

To date, techniques that have been considered as means of achieving reconfigurability include folding, such as self-deploying sun shields,[3)] assembly, such as formation flying and docking of individual spacecraft[4)] or assembly via robotic manipulation,[5)] and even 3D printing.[6)] However, self-reconfiguration of large 3D structures using these techniques remains a challenge. An alternative strategy can be drawn from the field of modular robotics, where structures are formed from individually actuated building blocks connected by temporary joints.[7)] In contrast to formation flying, reconfiguration without detachment precludes complex dynamics via a reduction of the degrees of freedom by imposing kinematic constraints similar to those leveraged by traditional deployable structures. Recently, robot collectives have demonstrated acquisition of target configurations via self-folding,[8)] and cubic robots have achieved self-reconfigurability in two dimensions via sliding[9)] and disassembly,[10)] and in three dimensions via pivoting.[11)] Moreover, a concept for self-assembly of modular spacecraft using flux-pinning magnet-superconductor pairs to form contact-less hinges has been successfully demonstrated in 2D experiments on air tables.[12,13)] While opposing moments due to gravity remain a challenge to the success and scalability of terrestrial reconfigurable robots, space offers an environment where even small forces can generate significant accelerations when integrated over sufficient timescales.

In this paper, we identify a novel concept for forming reconfigurable structures in space by using electromagnetically-actuated spacecraft, and base our design loosely on the PocketQube[14)] (PQ) in order to highlight the economic and technical challenges facing the construction of large reconfigurable structures today. We propose a design and deployment mechanism for a set of autonomous cubic spacecraft that acts a fully self-reconfigurable space structure and organize the paper as follows. We begin by introducing air-core electromagnetic coils as actuators between N neighbouring spacecraft, and simulate the forces generated for the chosen coil and spacecraft geometries. Second, we use Kane's method to symbolically derive the equations of motion for a multibody spacecraft system and introduce a controller that drives the collective to pivot between different configurations. As reconfiguration via pivoting requires all constituent modules to be in contact, we simulate N=8 unconnected

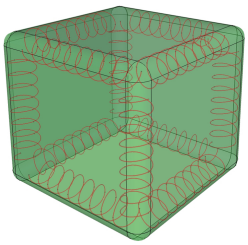

Fig. 1. EM coils are embedded along each edge of a cubic spacecraft to allow pivoting via electromagnetic actuation. Number of coil turns not to scale

spacecraft that are released in Low Earth Orbit (LEO) and aggregate into the initial configuration of a primitive cubic Bravais lattice (PCBL) via a behavioural path-planning technique. Finally, starting from this initial configuration, we simulate the full multibody dynamics and demonstrate reconfiguration from the PCBL into a line.

2. Concept overview

The resolution of the target structures being formed relies on large spacecraft numbers, and the launch and development costs associated with large collectives motivate miniaturization of the individual spacecraft. Among the smallest spacecraft with flight heritage today is the PQ, a cubic spacecraft with units characterized by a side length s of 50 mm and a mass of approximately 200 g. To date, four PQs have been launched,[15] the largest of which carried payloads including micro pulsed plasma thrusters and a camera. Of particular interest among these is the $50SAT PQ; while launched without a payload, it was manufactured for less than $250 in parts. More recently, a study by Cachia et al.[15] established that a constellation of 1-unit (1P) PQs with scientific payloads deployed in LEO is already a financially and technically practical proposition. Basing the defining physical characteristics of our system on today's technology, we model the spacecraft in our collective on the PQ and use as a starting point eight individual cubic spacecraft with side length 50 mm and mass 250 g deployed in LEO.

We use air-core electromagnets (EM) to actuate reconfiguration by pivoting neighbouring spacecraft relative to each other via both repulsion (pivot actuation) and attraction (hinge formation). EM actuators have previously been successfully used in pivoting mechanisms,[12] controlled formation flight[16] and docking[17] between neighbouring spacecraft. By embedding the edges of each spacecraft with independently controlled EMs (Fig. 1), the degree to which neighbouring spacecraft attract or repel can be regulated. By oppositely polarizing the edges of adjacent spacecraft, rigid face-to-face bonds can be made. Figure 2 demonstrates how pivoting is achieved by polarizing the EMs along the edge of one spacecraft such that they repel those of the adjacent edge, pivoting the spacecraft about the opposite edge whose oppositely polarized EMs create a hinge. By embedding EMs in all twelve edges of a cubic spacecraft, this single motion primitive gives rise to propellant-free self-reconfiguration via pivoting in three dimensions, while requiring no moving parts. By using EMs for hinge retention as well as actuation, it is conceptually feasible to achieve lubricant-free temporary hinges where opposing torques arise only from rolling friction, with no need for mechanical attachments between individual spacecraft.

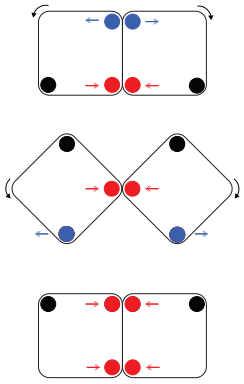

Fig. 2. Cross-section of two spacecraft performing a 180° pivot, with double-headed arrows indicating force direction. EM coils are displayed as circles that are undergoing attraction (red), repulsion (blue), or are unactuated (black). (Top) a first pair of EMs repel to initiate a pivoting maneuver, a second pair attract to form a hinge and a third pair is unactuated. (Middle) the first pair becomes unactuated, the second pair continues their attraction to maintain the hinge and the third pair begins repelling to decelerate the pivoting maneuver. (Bottom) the first pair remains unactuated, while the second and third pairs attract to form a rigid bond.

3. Force model

To maximize the forces available to pivot adjacent spacecraft, EMs are embedded along the inside of each spacecraft's twelve edges in order to minimize the separation distance between neighbouring EMs. As force scales proportionately with EM radius, EM radius is maximized to the extent that it becomes greater than the minimum separation between EMs in adjacent spacecraft. As a result, an analytical solution to the inter-EM forces is not available, as this relies on an approximation of the EMs as magnetic dipoles which is invalid for small inter-EM distances. Instead, we use Ampère's force law to consider the full geometries of the wires.

Ampère's force law shown in Eq. (1) gives the forces between two current-carrying conductors of arbitrary geometry by integrating the forces exerted on each element in one wire that arise due to the magnetic fields of each element in the other. The total force $F_{1,2}$ exerted on wire 1 due to wire 2 is expressed as a double line integral over each wire's geometry, where I_1 and I_2 are currents passing through wire elements of infinitesimal length $\mathrm{d}l_1$ and $\mathrm{d}l_2$ in wires 1 and 2, respectively, $\hat{r}_{12}$ is a unit vector from the elements on wire 1 to the elements on wire 2, r is the distance between these elements and μ_0 is the permeability of free space.

$$F_{1,2} = \frac{\mu_0}{4\pi} \int_1 \int_2 \frac{I_1 \mathrm{d}l_1 \times (I_2 \mathrm{d}l_2 \times \hat{r}_{12})}{\|r\|^2} \tag{1}$$

This equation has no known analytical solution and must be solved numerically. It is discretized to give Eq. (2), where D_1 and D_2 express the number of discretized elements in wire 1 and 2, respectively. The system dynamics are assumed to be slow and a quasi-static approximation holds.

$$F_{1,2} = \frac{\mu_0}{4\pi} \sum_{p=1}^{D_1} \sum_{q=1}^{D_2} \frac{I_p \mathrm{d}l_p \times (I_q \mathrm{d}l_q \times \hat{r}_{pq})}{\|r\|^2} \tag{2}$$

4. Dynamics and control

In this section, we present the derivation of the equations of motion used to relate EM forces to spacecraft accelerations. We then present a simple control strategy used to drive the pivoting maneuver.

4.1. Dynamic model

We use Kane's method[18] to derive the equations of motion of an N-spacecraft system symbolically. Kane's method is an alternative to the Lagrange and Newton-Euler methods to develop equations of motion. It is a vector-based approach that embeds both configuration constraints and motion constraints using generalized coordinates, and is particularly suited to the numerical computation of dynamics in large multibody systems.[19] Using the Sympy package[20] in Python, we develop the equations of motion for our multibody system in an automated way, making the implementation easily extendable for different choices of N. We leverage a special case that occurs when N spacecraft are constrained to only pivot about the N-1 hinges such that it forms a serial kinematic chain. In this case, reconfiguration of the system is tantamount to the control of an N-link pendulum.

Each spacecraft is modelled as a rigid body with equal mass that is uniformly distributed across the cubic geometry. We define a mechanical system with 7 mass-less links L_i connecting N=8 rigid bodies R_i consisting of point masses m_i with inertia J_i, moving in an inertial reference frame, where $i = [1..8]$. One spacecraft is defined with respect to the inertial frame using three states for position and three states for attitude expressed using Euler angles. The N-1 subsequent spacecraft in the kinematic chain are defined using 1 state representing a single rotation with respect to the former spacecraft, resulting in a total of 13 degrees of freedom (DoF) for an 8-body system. The locations of the twelve EMs $C_{i,k}$ of the ith spacecraft, where $k = [1..12]$, remain fixed in R_i. Forces $F_{C_{i,m},C_{i+1,n}}$ and $F_{C_{i,v},C_{i+1,w}}$ are applied bidirectionally between EMs in consecutive spacecraft i and $i+1$ for $m, n, v, w \in k$.

4.2. Control

From Eq. (2) we find that longitudinally aligned EMs (that is, with parallel axes) engender greater forces than axially aligned EMs; an intuitive result arising due to these achieving smaller separations and acting along the entire hinge of the spacecraft, rather than just one corner. To maximise power efficiency, we only actuate the two EM pairs furthest from the hinge as these provide the greatest moment arm at the beginning and end of the pivoting maneuver, where (m, n) and (v, w) represent the two pairs of EMs that initiate and complete the pivoting maneuver about the desired axis, respectively (Fig. 2). For clarity, we will refer to the EM pair (m, n) as the Pushing Pair (PP) and (v, w) as the Catching Pair (CP). As these EMs remain longitudinally aligned throughout the maneuver, the force that each EM exerts on the other is orientation-invariant in the rotational degree of freedom of the chosen hinge and can be computed as a function of the distance between them alone.

The requirement of the controller is twofold; to initiate the pivoting maneuver by imparting an angular acceleration between two adjacent spacecraft using control input U_{PP} acting between the PP, and to decelerate the spacecraft for a gentle conjoining upon completing the maneuver using control input U_{CP} acting between the CP.

Inputs U_{PP} and U_{CP} are used to set the product $I_1 I_2$ for the respective EM pair, as Eq. (2) shows that the distribution of the currents I_1 and I_2 between individual EMs is inconsequential. DC current control is employed and $I_1 I_2$ is limited to a maximum allowable current of $I_{max} = \max(U_{max,CP}, U_{max,PP})$. Furthermore, rolling friction and noise are neglected, and perfect knowledge of the system states is assumed to be available. For the control input U_{PP}, bang-bang control is used to initiate the maneuver using the maximum allowable input $U_{max,PP}$ as shown in Eq. (3):

$$U_{PP}(t) = \begin{cases} U_{max,PP} & e(t) = [e_{lim}, e_0] \\ 0 & e(t) = [0, e_{lim}) \end{cases} \tag{3}$$

where $e(t)$ is the error in radians at time t and e_0 is the error at time $t = 0$. This imparts maximum angular acceleration at the start of the maneuver when the tangential velocity vector is aligned with the force vector, and where $F_{1,2}$ is maximum due to minimum distance r between elements in PP. Input U_{PP} is then set to 0 once the limit e_{lim} has been reached, where e_{lim} is determined by choosing a value r at which $F_{1,2}/I_1 I_2$ becomes too small to warrant a continued supply of current. For the CP, proportional–integral–derivative (PID) control is used to set the desired control input U_{des} as shown in Eq. (4):

$$U_{des}(t) = k_p e(t) + k_i \int_0^t e(\tau) d\tau + k_d \frac{de(t)}{dt} \tag{4}$$

where k_p, k_i and k_d denote the gains for the proportional, integral and derivative terms, respectively, and a saturating element limits the desired control action U_{des} in order to keep input U_{CP} within maximum allowable inputs $\pm U_{max,PP}$ using Eq. (5):

$$U_{CP}(t) = \begin{cases} U_{max,CP} & U_{des}(t) \geq U_{max,CP} \\ U_{des}(t) & -U_{max,CP} < U_{des}(t) < U_{max,CP} \\ -U_{max,CP} & U_{des}(t) \leq -U_{max,CP} \end{cases} \tag{5}$$

Note that a negative $U_{max,CP}$ results in setting $I_1 I_2$ negative in Eq. (2), which is physically interpreted as oppositely polarizing EM coils 1 and 2. This simple method of achieving two-way actuation affords the controller far greater authority in the final approach than a unidirectional actuator can achieve.

A third control requirement for the reconfiguration concept is to maintain an electromagnetic hinge via a third EM pair at the axis of rotation. In formulating the dynamics as an N-link pendulum however, the hinges are enforced kinematically and hinge control is not necessary. Nonetheless, the minimum current necessary for hinge retention could be computed from the dynamics.

5. Initialization

Before reconfiguration of the collective can occur, the spacecraft must first be aggregated in space in an initial configuration. While one benefit of structural reconfigurability is that it affords leniency in this initial navigation and docking procedure, we propose and develop one method for acquiring particular target formations for completeness. Spacecraft homogeneity nullifies the need to pre-assign individuals among them to specific target positions. We therefore use an inverse dynamic and behaviour-based path planning technique called Equilibrium Shaping[21] (ES) that allows the spacecraft to solve the target assignment problem in a distributed manner amongst themselves, which it achieves by defining a kinematic field according to prescribed equilibrium points.

Starting from randomly initialized positions, ES allows N spacecraft—here also referred to as agents—to acquire a target configuration using distributed control and limited sensorial information. Specifically, we assume agents are able to determine their local attitude and compute inter-agent distances in order to obtain three-dimensional inter-agent relative position estimates. We also assume the spacecraft are able to deliver the required velocities using onboard thrusters.

5.1. Kinematical field design

The desired velocity field v_i^T of the ith agent is expressed as a weighted sum of three different behaviours named Gather (v_i^G), Avoid (v_i^A) and Dock (v_i^D) to give Eq. (6).

$$v_i^T = v_i^G + v_i^A + v_i^D \tag{6}$$

The objective of the Dock behaviour is to govern the agent velocities during the final approach by introducing N local attractors toward the N targets, where the Dock velocity of the ith agent is given by Eq. (7):

$$v_i^D = \sum_j d_j \psi_D(\left\|\zeta_j - P_i\right\|, k_D)(\zeta_j - P_i) \tag{7}$$

where P_i is the current position of the ith agent, ζ_j is the position of the jth target, d_j is a coefficient to be determined and ψ_D is a mapping from positive real numbers to positive real numbers that is a function of the tunable parameter k_D that sets the sphere of influence of the Dock behaviour.

In order to prevent collisions between spacecraft, the Avoid behaviour introduces a repulsive velocity term between agents given by Eq. (8):

$$v_i^A = \sum_j b \psi_A(\left\|P_i - P_j\right\|, k_A)(P_i - P_j) \tag{8}$$

where b is a coefficient to be determined and whose value is independent of j in order to maintain symmetry between agents, and where ψ_A is a mapping from positive real numbers to positive real numbers that is a function of the tunable parameter k_A that sets the sphere of influence of the Avoid behaviour.

By correctly tuning k_A and k_D, the spheres of influence are designed to only permit v_i^D and v_i^A to become non-negligible for agents in the near vicinity of targets or other agents, respectively, and the space is then considered flat. The role of the Gather behaviour v_i^G is to gather the N agents from any initial location in space by introducing N global attractors to the N targets. Therefore unlike v_i^D and v_i^A, it may need to act over large distances. As such, we design v_i^G to account for the gravitational field in order to exploit geodesics.

Considering each agent P_i as a chaser spacecraft trying to reach any target position ζ_j in a circular orbit about Earth, where Earth is considered a point mass, we write the closed form solution to the Clohessy-Wiltshire equations of motion in matrix form as:

$$\mathbf{P}(t) = [\mathbf{A}\ \mathbf{B}]\ [\mathbf{P_o}\ \dot{\mathbf{P}}_\mathbf{o}]^T \tag{9}$$

where $\mathbf{P}(t) = [x(t), y(t), z(t)]$ is the position of each agent with respect to the target-centered LHLV reference frame, $[\mathbf{P_o}\ \dot{\mathbf{P}}_\mathbf{o}] = [\mathbf{P}(0)\ \dot{\mathbf{P}}(0)]$ are the position and velocity at time $t = 0$, and matrices $\mathbf{A}$ and $\mathbf{B}$ are given by Eq. (10) and Eq. (11) respectively.

$$\mathbf{A} = \begin{bmatrix} 4 - 3\cos(nt) & 0 & 0 \\ 6(\sin(nt) - nt) & 1 & 0 \\ 0 & 0 & \cos(nt) \end{bmatrix} \tag{10}$$

$$\mathbf{B} = \begin{bmatrix} \frac{1}{n}\sin(nt) & \frac{2}{n}(1 - \cos(nt)) & 0 \\ \frac{2}{n}(\cos(nt) - 1) & \frac{1}{n}(4\sin(nt) - 3nt) & 0 \\ 0 & 0 & \frac{1}{n}\sin(nt) \end{bmatrix} \tag{11}$$

where $n = \sqrt{\frac{\mu}{a^3}}$, μ is the gravitational constant and a is the orbital altitude. Solving Eq. (9) for velocity, we can then define a gather velocity $v_i^{G,gr}$ that accounts for gravity as Eq. (12):

$$v_i^{G,gr} = \frac{1}{N} \sum_j \mathbf{B}^{-1}\zeta_j - \mathbf{B}^{-1}\mathbf{A}P_i \tag{12}$$

where $\mathbf{A} = \mathbf{A}(t_d - t)$, $\mathbf{B} = \mathbf{B}(t_d - t)$ and t_d is the time in which the agent should complete the rendezvous. As Eq. (12) becomes singular when t_d approaches t, we introduce a second gather term $v_i^{G,fl}$ for the final approach of the rendezvous. Leveraging the fact that $\left\|\zeta_j - P_i\right\|$ approaches 0 as t_d approaches t, this behaviour assumes the space is flat and is given as:

$$v_i^{G,fl} = \sum_j c_j \psi_G(\left\|\zeta_j - P_i\right\|)(\zeta_j - P_i) \tag{13}$$

where c_j is a coefficient to be determined and ψ_G is a mapping from positive real numbers to positive real numbers that can be used to introduce non-linear dependencies on the distance to the target. Finally, we define v_i^G as the piecewise function in Eq. (14):

$$v_i^G = \begin{cases} v_i^{G,fl} & \left\|\zeta_j - P_i\right\| < R_G \\ v_i^{G,gr} & \left\|\zeta_j - P_i\right\| \geq R_G \end{cases} \tag{14}$$

where R_G is the radius of a sphere centered on the targets that marks the transition between the gather behaviours.

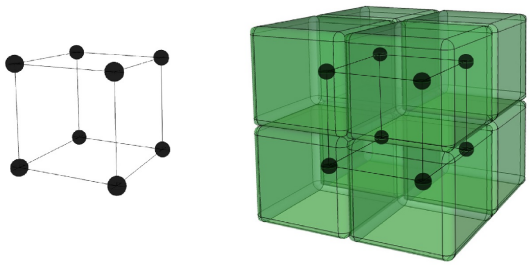

Fig. 3. (Left) a primitive cubic Bravais lattice. (Right) eight spacecraft having acquired their target configuration, where each spacecraft is centered on one node of the lattice.

6. Equilibrium Shaping

Here we derive the ES formula for N=8 randomly initialized agents given the task of acquiring the target spatial configuration of a PCBL as shown in Fig. 3. The ES technique exploits symmetry in the PCBL to form equilibria equations, and of the admissible configurations available to ES, a primary driver for selecting the PCBL arises from an intriguing possibility to assemble cube-shaped spacecraft into cube-based lattices recursively in an octree structure for large N.

We begin by setting the functions ψ_D, ψ_A and ψ_G for the behaviours in the vicinity of the target formation:

$$\psi_D(\left\|\zeta_j - P_i\right\|, k_D) = e^{-\frac{\left\|\zeta_j - P_i\right\|^2}{k_D}} \tag{15}$$

$$\psi_A(\left\|P_i - P_j\right\|, k_A) = e^{-\frac{\left\|P_i - P_j\right\|^2}{k_A}} \tag{16}$$

$$\psi_G(\left\|\zeta_j - P_i\right\|) = 1 \tag{17}$$

These equations show that when the inverse exponential terms $\left\|\zeta_j - P_i\right\|$ and $\left\|P_i - P_j\right\|$ are large (i.e. spacecraft are far from the targets and other agents, respectively), ψ_D and ψ_A become negligible and $v_i^G \gg v_i^D, v_i^A$. This allows the Gather behaviour to dominate Eq. (6) and the agents will move towards the center of mass of the targets. On the other hand, when $\left\|\zeta_j - P_i\right\|$ and $\left\|P_i - P_j\right\|$ are small, v_i^D and v_i^A dominate Eq. (6), respectively.

In order to enforce the particular equilibria for the PCBL, we re-write Eq. (6) as the dynamical system in Eq. (18) and determine the coefficients $\lambda = [c_j, d_j, b]$ satisfying this under the condition presented in Eq. (19) that shows the agents having acquired the target formation as in Fig. 3. This gives the dynamical system equilibrium points for all possible agent permutations in the target configuration.

$$\dot{P} = v_i^T = f(P, \zeta, \lambda) \tag{18}$$

$$f(P = \zeta, \zeta, \lambda) = 0 \tag{19}$$

Introducing $\Omega(\left\|\zeta_j - P_i\right\|) = \dot{P}$ and assuming Eq. (19) is satisfied, we choose an agent located at any target node of the PCBL and evaluate $\Omega(\left\|\zeta_j - P_i\right\|)$ using Eq. (19) to find seven non-zero terms corresponding to the seven remaining nodes. We decompose these terms into the three orthogonal axes aligned with the PCBL's edges and set equal to 0 to find Eq. (20):

$$\Omega(L)L + 2\Omega(L\sqrt{2})L + \Omega(L\sqrt{3})L = 0 \tag{20}$$

where L is the length of one side of the PCBL. By symmetry, we find the Equilibrium Shaping formula reduces to one scalar relation, which holds for any node chosen as the starting point. Substituting ψ_D, ψ_A and ψ_G into Eq. (20) and rearranging, we find Eq. (21) for $c_j = c$ and $d_j = d$, giving a relation between parameters b, c and d for which the dynamical system has the PCBL nodes as its equilibrium points.

$$c = \frac{b}{4}(e^{-\frac{L^2}{k_A}} + 2e^{-\frac{2L^2}{k_A}} + e^{-\frac{3L^2}{k_A}}) - \frac{d}{4}(e^{-\frac{L^2}{k_D}} + 2e^{-\frac{2L^2}{k_D}} + e^{-\frac{3L^2}{k_D}}) \tag{21}$$

7. Results

7.1. Force model

The force model is verified using the Far Field model in Eq. (22), a linearized model that approximates the EMs as magnetic dipoles rather than rings of current, and is only valid when the EMs are separated by more than 6-8 coil radii.[22] For axially aligned EMs, the Far Field force (F_{FF}) is expressed as:

$$F_{FF} = \frac{3\mu_0}{2\pi}\frac{\mu_F^2}{d_{12}^4} \tag{22}$$

where d_{12} is the distance separating the coil centers and the coil parameter $\mu_F = \pi R_c^2 N_F \sqrt{I_1 I_2}$ is evaluated using radius R_c = 4 mm and 200 turns (N_F). Computing Eq. (2) and Eq. (22) for axially aligned EMs of length L_c = 34 mm separated by distance d_{12} in the range $[8R_c, 100R_c]$ in increments of $0.2R_c$, we find that for D_1, D_2 = 3000, our model correlates with the Far Field model to within 1%.

For each longitudinally aligned EM pair PP and CP, forces are decomposed along the separation axis F_s, coil axis F_c, and a third axis F_h that completes the orthogonal system, and are computed for linear separations along the separation axis in the range [0,100] mm in increments of 0.2 mm. As this calculation is computationally expensive, it is computed offline and fitted with a function that can be used in the dynamic simulation. In particular, we find that $F_s \gg Fc, Fh$, so that neglecting F_c, F_h our fitted force equation reduces to F_s given by Eq. (23).

$$F_s = 3I_1 I_2 d_{12}^{-2.299} \times 10^{-9} \tag{23}$$

We therefore set $F_{C_{i,m},C_{i+1,n}}$ and $F_{C_{i,v},C_{i+1,w}}$ equal to F_s, i.e. only electromagnetic forces induced along the separation axis are considered. This function gives a coefficient of determination with the model of 0.9998 in the range [2,20] mm where forces are largest, and where a 2 mm lower bound is selected as the smallest possible separation between adjacent EMs given a spacecraft wall thickness of 1 mm. Due to the rapid decay of EM force with distance, we neglect cross-coupled forces exerted by the PP on the CP and vice versa.

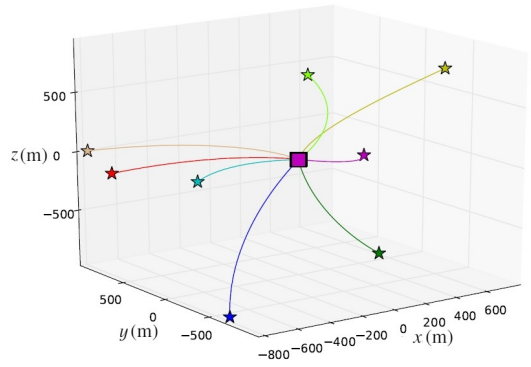

Fig. 4. Eight spacecraft initialized at random locations (starred markers) follow geodesic trajectories during the initial descent toward the target destination (square markers). Markers not to scale.

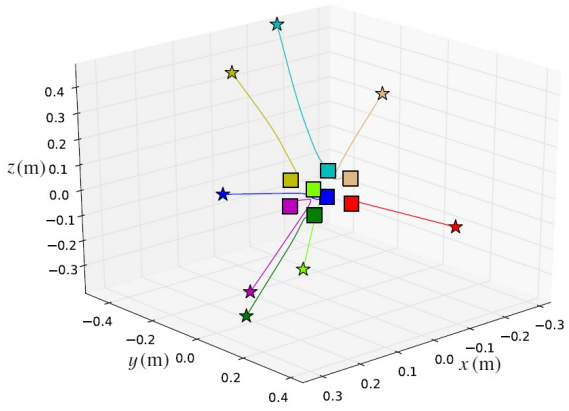

Fig. 5. Trajectories of the eight spacecraft on the final approach before acquisition of the target formation (square markers), for which the spacecraft occupy the PCBL nodes. Markers not to scale.

7.2. Assembly

We simulate eight spacecraft initialized with zero velocity in positions uniformly distributed across a sphere of radius 1000 m around a target location in LEO, at an orbital altitude of 415 km and with the transition radius R_G set to 1 m. A total assembly time of 200 minutes was achieved for parameters $b = 1, d = 0.5$ and $k_A, k_D = 0.1$, resulting in a value for c of 0.0860421 for which the spacecraft successfully reach all targets in the PCBL.

Figure 4 shows the initial trajectories of the spacecraft with velocities set to $v_i^{G,gr}$ to account for the gravitational influence of the Earth and integrated at 0.125 Hz. Figure 5 shows the final approach of the spacecraft, where the spacecraft use $v_i^{G,fl}$ to follow trajectories that assume a flat space in the vicinity of the target, and where the integration rate has been increased to 2 Hz. Under this final approach, each spacecraft closes a final distance of approximately 0.3 m in 150 seconds to correctly settle on the nodes of the PCBL of side length 0.1 m. This permits the 0.05 m side length spacecraft to perfectly align when centered on the nodes as shown in Fig. 3.

The ES parameters were chosen to achieve assembly in desired timescales, consideration was not given to the thrusters or control strategies necessary to achieve these velocities. Moreover, the parameter choices were tuned by trial and error, and a number of permutations were found that led to configurations with local minima for which the spacecraft failed to reach the target configuration.

7.3. Reconfiguration

We compute the symbolic equations of motion of the multibody system using the physical parameters $m_i = 250$ g, $s = 50$ mm and $J_i = m_i s^2/6$, while $\|L_i\|$ reflects the distance between the center of one EM and the next and so varies depending on the location of consecutive hinges in 3D space.

In setting the current limits, we use an analysis by Cachia et al.[15] that outlines the design of an electrical power system (EPS) of a 1P PQ in LEO capable of supplying a daily average of 300 mW and a peak output of 1660 mW after accounting for typical EPS efficiencies. For the chosen EM geometry, the DC resistance of the EM is 1.16 Ω for a copper coil of resistance 1.68×10^{-8}Ωm with a rectangular cross-section of height 0.17 mm and an aspect ratio of 2.5. In the worst case, control inputs will saturate to $U_{max,CP}$ and $U_{max,PP}$ for the duration of the pivot, and the worst case current required for one spacecraft undergoing a 180° pivot is $\sqrt{U}_{max,CP} + \sqrt{U}_{max,PP}$ for equally distributed currents I_1 and I_2 between EMs in each EM pair. Assuming that maneuvers can be performed using a hinge current less than or equal to this sum, it is multiplied by 2 to account for the un-modeled hinge current and the result is multipied by 1.16 Ω to give a power estimate of the pivot maneuver. Choosing $U_{max,CP} = 0.13$ and $U_{max,PP} = 0.12$ satisfies $U_{max,CP} \geq U_{max,PP}$ to mitigate collisions resulting from overshoot in simple systems and yields a total power requirement of 1650 mW ≤ 1660 mW.

7.3.1. Controller performance

The controller is tuned heuristically and the step response of a 2-body system to a 180° pivot is shown for clarity in Fig. 6, where $k_p = -5, k_d = -350, k_i = -0.03, e_{lim} = e_0/2$ and the controller runs at 60 Hz. A simulation of the two cubes highlighting their orientations is superimposed on coordinate axes and displayed at the top of Fig. 6 at the corresponding time, where the position of the hinge is tracked using an orange square. The pivot maneuver is completed in 233 seconds, with a rise time of 151 seconds and a steady state error 0.05°. A large k_d was required to conservatively over-damp the system to ensure a soft final collision and mitigate instabilities. For small values of k_d, the spacecraft reach the setpoint at significant speeds and a large repulsive force induces an acceleration away from the setpoint that cannot reversed due to the rapid decay of the force function with distance and the limit ($U_{max,CP}$) imposed on the controller. Conversely, k_p exhibits a near negligible effect on the system, contributing a large component to the input for high error values when the induced force is small, while contributing only a small component to the input for small error values where the force induced would be more significant. The resulting k_d-dominated behaviour of U_{CP} acts to attract the spacecraft when the error is large, before saturating from its negative limit to its positive limit as the relative angular velocity of the spacecraft rises. While allowing a negative input on U_{CP} permits the pair to attract during the initial phase of the maneuver, future designs that consider power constraints more rigorously should set this to 0 for large errors in the way U_{PP} is set to 0 for small errors, under which conditions the forces that the respective EM pairs can exert become negligible.

From the above, the 2-body system from Fig. 6 is capable

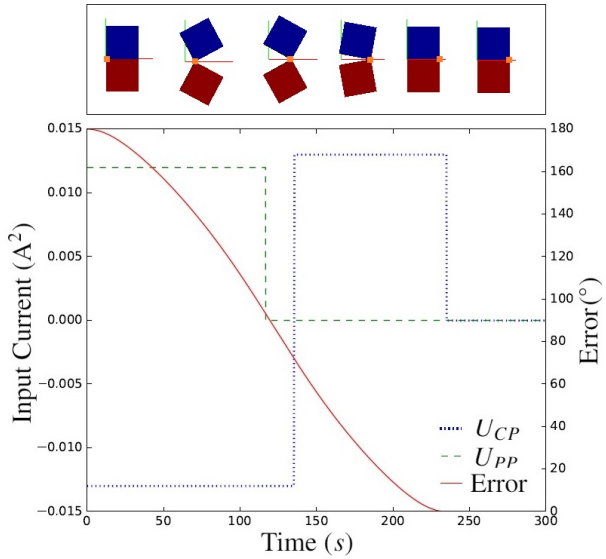

Fig. 6. Two spacecraft undergoing a 180° pivot. (Top) simulation of the maneuver with the hinge tracked in orange. (Below) step response showing error and input current during the maneuver. Input current U_{CP} sets $I_1 I_2$ for the Catching Pair and is determined using PID control, while input current U_{PP} sets $I_1 I_2$ for the Pushing Pair using bang-bang control.

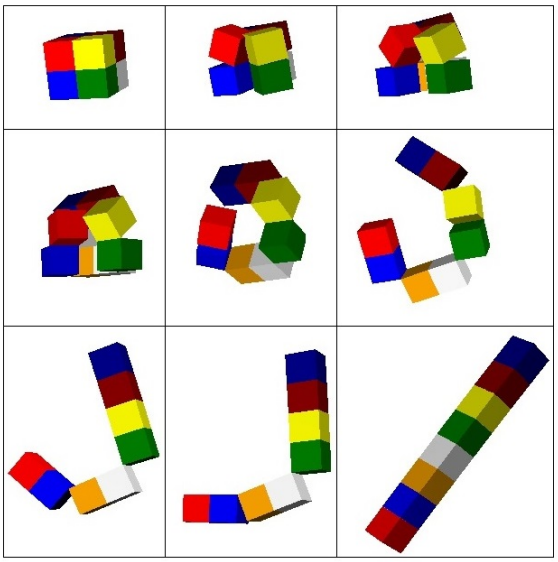

Fig. 7. Eight spacecraft initialized in the formation of a primitive cubic Bravais lattice (top left) reconfigure into a line (bottom right).

of completing a maximum of 67 pivot maneuvers each day, for maneuvers that require 1650 mW for 233 seconds and given an available average power of 300 mW/day. This number halves for a 2-body system in which one mass m_i is replaced with a mass M set to $M = \infty$, and lies between these two limits for the general case of a mass m_i pivoting with respect to a non-pivoting N-body system with zero initial angular momentum of mass M, where $m_i < M < \infty$.

7.3.2. Multibody simulation

Provably correct reconfiguration algorithms for pivoting cubes recently developed by Sung et al.[23] have achieved transitions between arbitrarily configured 3D lattices in under $O(n^2)$ moves, barring three inadmissible sub-configurations. This algorithm utilizes a proof showing that any two admissible configurations can reconfigure into a line, and that these two configurations can therefore reconfigure into each other via first transitioning to an intermediary line configuration. To the authors' knowledge, this is the only algorithmic study of pivoting cubes in three dimensions and is conducted without consideration of the underlying physics. As a result, we demonstrate our controller's ability to reconfigure a system of eight cubic spacecraft from their initial configuration in the PCBL into a line while simulating the full dynamics of the system. We use an asymmetric pivoting pattern and asynchronous pivoting order in order to highlight the dynamics of the system, and show snapshots of the reconfiguration in Fig. 7. The generation and integration of the equations of motion takes 26 minutes on a Windows machine (64-bit, Intel Core i7, 8 GB RAM). The equations of motion contain 1704176 individual occurrences of the state variables, underscoring the need for automating the generation of symbolic equations of motion for large multibody systems.

The controller was successfully implemented on the multibody system without gain scheduling, reconfiguring the eight spacecraft in Fig. 7 in 1800 seconds. However, this assembly time varied significantly with the order and timing of the individual pivoting maneuvers. These inconsistencies arise primarily due to the time dependence of the system's inertia that results from the order and timing of the individual maneuvers. The particular order and timing choices that led to successful simulations were found heuristically, while other permutations led to a failure of the system to acquire the line configuration in reasonable timescales altogether. These failures occur when a pivoting maneuver becomes stalled mid-pivot due to motion from other pivoting maneuvers in the kinematic chain, and where the distances between EM pairs are too large for the forces to generate significant further acceleration. However, these failures were easily mitigated either by assembling spacecraft one by one from one end of the kinematic chain or by increasing I_{max} to raise the maximum allowable controller inputs.

It can also be noted that two pairs of spacecraft remain in their initial subconfigurations for the duration of the simulation in order to highlight the possibility of metamodule reconfiguration—that is, to use EMs to form temporary bonds that allow maneuvering of several spacecraft as a single entity. Rather than pivoting each individual spacecraft one by one, this further increases the space of possible maneuvers that can be selected in transitioning between configurations.

8. Discussion

In this paper we have proposed and outlined a novel framework for achieving reconfigurable space structures using a robotics-inspired approach. In particular, we have introduced simple electromagnetic coils as a means of pivoting neighbouring spacecraft with respect to each other. For this a force model of the electromagnetic actuators was developed using Ampère's force law and verified using the Far Field model. Furthermore, these electromagnetic actuators provide each spacecraft with self-aligning low-mass connectors capable of forming temporary bonds with their neighbours. These connectors are moreover orientation-invariant, genderless, quick to engage and tol-

erant to misalignment. On the other hand, they exhibit relatively low strength, draw power while engaged and dissipate heat during operation. Future work could include the design of a mechanical latch to allow forming permanent bonds between neighbouring spacecraft, as well as substituting or complementing the EMs with electropermanent[10] magnets that allow switchable electromagnetic adhesion without power consumption. Of particular interest to the authors is the possibility to overload the EMs with additional functionality such as inductive wireless power transmission between neighbouring spacecraft. This could allow non-contact power sharing between spacecraft without protruding parts or physical electrical connections, in addition to allowing communication and information transmission in the collective.

The generation of symbolically expressed equations of motion was automated for eight daisy-chained cubic spacecraft, allowing for rapid computation and limiting the susceptibility of the derivation to human error. A controller was simulated capable of achieving pivoting maneuvers subject to hypothetical constraints on power. Reconfigurations were successfully demonstrated using heuristically tuned controller gains for 180° pivots on 2-body and 8-body systems. For the 8-body system, a simulation demonstrated reconfiguration from the initial shape of a PCBL into a line, motivated by utilizing recently developed provably correct algorithms for pivoting cubes[23] while modelling the full dynamics of the system. One limitation of formulating the problem as a kinematic chain is in its inability to allow traversal maneuvers, however an extension could be implemented to allow this by updating kinematic constraints online. While the controller performed sufficiently well for small systems, sensor noise has been neglected and perfect knowledge of the system states was assumed. In future implementations, knowledge of the model could be leveraged to better handle changes in inertia in the system and to optimize the input for power and assembly time.

The ability of one spacecraft to perform 34 pivot maneuvers per day while attached to a larger non-rotating structure in LEO suggests that integrating EM actuators into a collective of PocketQube could allow significant reconfigurability of the collective. While the force model and dynamical model used to arrive at this result underwent significant simulation and modelling, more lenient assumptions were made to estimate the power required for hinge retention. Additional factors to consider in future work include depth of discharge and the occlusion of solar panels by other spacecraft, however any further limits to the available peak power can be traded for longer pivot times.

While reconfigurability should preclude the need for a particular initial configuration, a method for aggregating the spacecraft in an initial configuration was proposed and simulated using the ES technique.[21] As a distributed path planning technique that relies on limited sensorial information, ES is suited for swarm applications with many agents as envisioned in this paper. Starting from a randomly initialized 8-spacecraft swarm, ES is used to successfully acquire a target configuration of a PCBL that moreover exploits geodesic trajectories during the initial descent toward the targets. The symmetry between the choice of lattice and shape of each spacecraft moreover presents an opportunity to assembly cube-shaped spacecraft into cube-based lattices recursively in an octree structure for larger systems. The spacecraft velocities found by ES are set without consideration for the underlying dynamics, thus a beneficial extension of this work would include exploring candidate thrusters and control strategies for the aggregation phase. Of particular interest is the control of spacecraft pose during the final approach, where EMs themselves may be used to complete the final assembly; this proposition is corroborated by the accidental magnetic conjunction of cubesats HRBE and MCubed in 2011, which is hypothesized to have occurred due to the attraction between onboard permanent magnets intended for passive attitude control.[24]

9. Conclusion

This paper has introduced a conceptual framework for achieving on-orbit formation of reconfigurable space structures using individually actuated electromagnets embedded in the edges of large swarms of miniature spacecraft that are based on the PocketQube. A behaviour-based and distributed path planning technique called Equilibrium Shaping was used to successfully assemble eight spacecraft in an initial configuration in LEO. Using automatically generated equations of motion, we demonstrate the first controlled transition from this initial configuration to a target configuration using pivoting 3D cubes that considers the underlying physics of the system. Finally, a heuristically tuned PID controller was found that successfully drives pivoting maneuvers for small $N \leq 8$ multibody spacecraft systems, however future larger systems will require more stringent constraints on pivoting order and consideration for simultaneous maneuvers in the system.

References

1) Craig Underwood, Sergio Pellegrino, Vaios J Lappas, Christopher P Bridges, and John Baker. Using cubesat/micro-satellite technology to demonstrate the autonomous assembly of a reconfigurable space telescope (aarest). *Acta Astronautica*, 114:112–122, 2015.
2) WR Oegerle, LR Purves, JG Budinoff, RV Moe, TM Carnahan, DC Evans, and CK Kim. Concept for a large scalable space telescope: In-space assembly. In *SPIE Astronomical Telescopes+ Instrumentation*, pages 62652C–62652C. International Society for Optics and Photonics, 2006.
3) Lee Wilson, Sergio Pellegrino, and Rolf Danner. Origami sunshield concepts for space telescopes. In *54th AIAA/ASME/ASCE/AHS/ASC Structures, Structural Dynamics, and Materials Conference*, page 1594, 2013.
4) CY Xia, PK C. Wang, and FY Hadaegh. Optimal formation reconfiguration of multiple spacecraft with docking and undocking capability. *Journal of guidance, control, and dynamics*, 30(3):694–702, 2007.
5) Nicolas Lee, Paul Backes, Joel Burdick, Sergio Pellegrino, Christine Fuller, Kristina Hogstrom, Brett Kennedy, Junggon Kim, Rudranarayan Mukherjee, Carl Seubert, et al. Architecture for in-space robotic assembly of a modular space telescope. *Journal of Astronomical Telescopes, Instruments, and Systems*, 2(4):041207–041207, 2016.
6) TJ Prater, QA Bean, RD Beshears, TD Rolin, NJ Werkheiser, EA Ordonez, RM Ryan, and FE Ledbetter III. Summary report on phase i results from the 3d printing in zero g technology demonstration mission, volume i. 2016.
7) Daniela Rus and Marsette Vona. Crystalline robots: Self-reconfiguration with compressible unit modules. *Autonomous Robots*, 10(1):107–124, 2001.
8) Martin EW Nisser, Samuel M Felton, Michael T Tolley, Michael Rubenstein, and Robert J Wood. Feedback-controlled self-folding

of autonomous robot collectives. In *Intelligent Robots and Systems (IROS), 2016 IEEE/RSJ International Conference on*, pages 1254–1261. IEEE, 2016.

9) Byoung Kwon An. Em-cube: cube-shaped, self-reconfigurable robots sliding on structure surfaces. In *Robotics and Automation, 2008. ICRA 2008. IEEE International Conference on*, pages 3149–3155. IEEE, 2008.
10) Kyle Gilpin, Kent Koyanagi, and Daniela Rus. Making self-disassembling objects with multiple components in the robot pebbles system. In *Robotics and Automation (ICRA), 2011 IEEE International Conference on*, pages 3614–3621. IEEE, 2011.
11) John W Romanishin, Kyle Gilpin, Sebastian Claici, and Daniela Rus. 3d m-blocks: Self-reconfiguring robots capable of locomotion via pivoting in three dimensions. In *Robotics and Automation (ICRA), 2015 IEEE International Conference on*, pages 1925–1932. IEEE, 2015.
12) William Wilson, Joseph Shoer, and Mason Peck. Demonstration of a magnetic locking flux-pinned revolute joint for use on cubesat-standard spacecraft. In *AIAA Guidance, Navigation, and Control Conference*, page 5904, 2009.
13) Joseph Shoer and Mason Peck. Reconfigurable spacecraft as kinematic mechanisms based on flux-pinning interactions. *Journal of Spacecraft and Rockets*, 46(2):466–469, 2009.
14) Stefano Speretta, Mrs Tatiana Perez Soriano, Mr Jasper Bouwmeester, Mr Johan Carvajal-Godinez, Alessandra Menicucci, Mr Trevor Watts, Mr Prem Sundaramoorthy, Jian Guo, and Eberhard Gill. Cubesats to pocketqubes: Opportunities and challenges. 2016.
15) Darren Cachia, Jonathan Camilleri, Marc Anthony Azzopardi, Matthew Angling, and Andrew Sammut. Feasability study of a pocketqube platform to host an ionospheric impedance probe.
16) Allison K Porter, Dustin J Alinger, Raymond J Sedwick, John Merk, Roedolph A Opperman, Alexander Buck, Gregory Eslinger, Peter Fisher, David W Miller, and Elisenda Bou. Demonstration of electromagnetic formation flight and wireless power transfer. *Journal of Spacecraft and Rockets*, 51(6):1914–1923, 2014.
17) Yuan-wen Zhang, Le-ping Yang, Yan-wei Zhu, Huan Huang, and Wei-wei Cai. Nonlinear 6-dof control of spacecraft docking with inter-satellite electromagnetic force. *Acta Astronautica*, 77:97–108, 2012.
18) Thomas R Kane and David A Levinson. *Dynamics, theory and applications*. McGraw Hill, 1985.
19) Ronald Huston. Multibody dynamics formulations via kane's equations. In *Orbital Debris Conference: Technical Issues andFuture Directions*, page 1234, 1990.
20) Aaron Meurer, Christopher P. Smith, Mateusz Paprocki, Ondřej Čertík, Sergey B. Kirpichev, Matthew Rocklin, AMiT Kumar, Sergiu Ivanov, Jason K. Moore, Sartaj Singh, Thilina Rathnayake, Sean Vig, Brian E. Granger, Richard P. Muller, Francesco Bonazzi, Harsh Gupta, Shivam Vats, Fredrik Johansson, Fabian Pedregosa, Matthew J. Curry, Andy R. Terrel, Štěpán Roučka, Ashutosh Saboo, Isuru Fernando, Sumith Kulal, Robert Cimrman, and Anthony Scopatz. Sympy: symbolic computing in python. *PeerJ Computer Science*, 3:e103, January 2017.
21) Dario Izzo and Lorenzo Pettazzi. Autonomous and distributed motion planning for satellite swarm. *Journal of Guidance, Control, and Dynamics*, 30(2):449–459, 2007.
22) Samuel Adam Schweighart. *Electromagnetic formation flight dipole solution planning*. PhD thesis, Massachusetts Institute of Technology, Department of Aeronautics and Astronautics, 2005.
23) Cynthia Sung, James Bern, John Romanishin, and Daniela Rus. Reconfiguration planning for pivoting cube modular robots. In *Robotics and Automation (ICRA), 2015 IEEE International Conference on*, pages 1933–1940. IEEE, 2015.
24) John C Springmann, Andrew Bertino-Reibstein, and James W Cutler. Investigation of the on-orbit conjunction between the mcubed and hrbe cubesats. In *Aerospace Conference, 2013 IEEE*, pages 1–8. IEEE, 2013.